Molecular layer interneurons in the cerebellum encode for valence in associative learning

Ming Ma[1,2], Gregory L. Futia[3], Baris N. Ozbay[4], Emily A. Gibson[3] and Diego Restrepo[1,2,*]

[1] Neuroscience Graduate Program

[2] Department of Cell and Developmental Biology

[3] Department of Bioengineering

University of Colorado Anschutz Medical Campus, Aurora, CO 80045, USA

[4]Intelligent Imaging Innovations, Denver, CO, 80216.

[*]Corresponding author: Diego Restrepo, diego.restrepo@cuanschutz.edu

Abstract

We used two-photon microscopy to study the role of ensembles of cerebellar molecular layer interneurons (MLIs) in a go-no go task where mice obtain a sugar water reward if they lick a spout in the presence of the rewarded odorant and avoid punishment when they restrain from licking for the unrewarded odorant. When the animal was naïve to the valence of the stimulus (is the odorant rewarded?) responses of the MLIs did not differ between odorants. However, as the animal became proficient, the rewarded odorant elicited a large increase in Ca^{2+} in MLIs, and the identity of the odorant could be decoded from the differential response. Importantly, MLIs switched odorant responses when the valence of the stimuli was reversed. Finally, licks diverged more slowly and mice did not become proficient when MLIs were inhibited by chemogenetic intervention. Our findings support a role for MLIs in learning valence in the cerebellum.

Introduction

The cerebellum plays a pivotal role in coordinating movements through sensorimotor integration. It receives massive input through mossy fiber (MF) synapses onto granule cells (GCs) to form a circuit efficient in complex pattern separation[1] (Supplementary Fig. 1). In addition, the cerebellum contributes to non-motor processes such as cognition and emotion and is associated with non-motor conditions such as autism spectrum disorders[2-5]. The Purkinje cells (PCs), the sole projection neurons of the cerebellar cortex, receive excitatory afferent input from the parallel fibers (PFs) of GCs and dense feedforward inhibitory inputs from the molecular layer interneurons (MLIs). Importantly, subtle changes in this PC excitatory-inhibitory balance generate robust, bidirectional changes in the output of PCs[6].

Plasticity in cerebellar circuit activity plays an important role in generation of adequate motor output. Indeed, long term depression (LTD) mediated by dendritic increases in Ca^{2+} in PCs elicited by motor error signals conveyed by climbing fibers (CFs) is a classical model of plasticity in the cerebellar circuit[7-10]. However, recent studies indicate that CFs also signal reward prediction[11,12] or decision-making errors[13], and the cerebellum modulates association pathways in the ventral tegmental area (VTA) enabling a cerebellar contribution to reward-based learning and social behavior[14]. Interestingly, MLIs have been proposed to participate in cerebellar plasticity[15-17], and Rowan and co-workers found graded control of PC plasticity by MLI inhibition[18] suggesting that MLI inhibition is a gate for learning stimulus valence (contextual identity, is the stimulus rewarded?). However, whether there is a causal participation of MLIs in reward-associated learning is unknown.

Here we explored whether MLI activity plays a role in reward-associated learning in a go-no go task where the thirsty animal learns to perform sustained licking to obtain a water reward [19,20]. We applied two-photon microscopy[21] to record Ca^{2+} changes in ensembles of lobule VI MLIs expressing GCaMP[22] during the self-initiated go-no go learning task. To test the sufficiency of interneuron activity for associative learning, we utilized DREADD chemogenetics[23] to determine whether local inhibition of MLI activity elicited changes in learning.

Results

In order to explore the role of MLIs in associative learning we employed *in vivo* two-photon microscopy to record neural activity reported by changes in fluorescence emitted by the cytosolic Ca^{2+} indicators GCaMP6/7. MLIs were imaged in head-fixed mice through a 2x2 mm glass window implanted above the cerebellar vermis (lobule VI, Fig. 1, Supplementary Fig. 2), an area of the cerebellum where GCs acquire a predictive feedback signal or expectation reward[24,25]. We used the go-no go task where thirsty mice receive a water reward when they lick in response to a rewarded odorant (1% isoamyl acetate, Iso, termed S+) (Fig. 1a, Hit trial, mouse movement is shown in Supplementary Movie 1 and quantified in Supplementary Fig. 3). Mice did not receive the reward if they failed to lick (Miss trial). When the unrewarded odorant was presented (S- trials) the animals did not receive a reward when they refrained from licking (Correct Rejection, CR, Fig. 1a), and they were punished with a timeout of ten seconds if they licked (False Alarm, FA).

Figs. 1bi,ii show an example of an increase in MLI GCaMP6f fluorescence intensity elicited in a Hit trial for a mouse proficient discriminating between the stimuli (we define proficient as >=80% correct in a twenty trial window). We extracted regions of interest (ROIs) of the components (Fig. 1biii) and temporal traces of the normalized change in fluorescence ($\Delta F/F$, Fig. 1c and d) using constrained nonnegative matrix factorization analysis[26]. Fig. 1d shows time courses for $\Delta F/F$ for 20 selected ROIs and licks (blue trace at the bottom, vertical red and blue lines indicate odorant on and off times for the S+ and S- trials respectively). MLIs responded to the rewarded odorant with substantial increases

in Ca^{2+} and smaller changes to the unrewarded odorant (with exceptions, see arrow). The mouse licked during the S+ trials (and sparsely for most of the S- trials). Finally, Fig. 1c shows the average per trial changes in ΔF/F for Hit (i) and CR (ii) for all components in this example. The magnitude of the normalized change in ΔF/F of Hit trials is larger than in CR trials.

Cerebellar MLIs develop divergent responses as mice learn to differentiate odorants. Fig. 2a shows the behavioral performance in a learning session where the animal reached proficient level (>80%) after 70 trials. Fig. 2b shows the time course per trial for ΔF/F for S+ and S- stimuli for this session (mean over all ROIs±95% confidence interval, CI). In addition, Figs. 2c and d show mean ΔF/F computed per trial for a one second period before odorant addition (pre-odorant, Fig. 2c) and for the last second of the odorant period (Fig. 2d). For this session we observed small differences between the S+ and S- for the ΔF/F time courses when the animals were performing <65% correct (Fig. 2bi). As the animal learned to differentiate the odorants (65-80% and >80% percent correct, Figs. 2bii and iii), a differential response developed with no overlap between the bootstrapped confidence intervals. For S+ trials ΔF/F started increasing at trial initiation (1-1.5 sec before odorant addition) and reached a peak when the animal was rewarded, while for S- trials, the response returned to basal levels shortly after the odorant was applied. Fig. 2f shows the mean ΔF/F (±CI) for the last second of odorant application for trials falling within different percent correct performance ranges (Supplementary Fig. 4). A generalized linear model (GLM) analysis finds a statistically significant interaction between performance and the odorant (S+ vs. S-) ($p<0.001$, 44 d.f., 4 mice). Therefore, as the animal learns the change

in Ca^{2+} in MLIs diverges between S+ and S- odorants, suggesting a possible role for MLIs in associative learning.

Finally, we calculated the dimensionality of ΔF/F responses for the MLI cell ensemble. The plots in Fig. 1c indicate that odorant responses are fairly uniform for the ROIs in the FOV. In order to provide an estimate of the number of independent components comprising the ΔF/F responsiveness of the ensemble we calculated a quantitative measure of dimensionality[27] (see Methods). Fig. 2g shows the dimensionality for four sessions with a total number of ROIs ranging from 103 to 136. The dimensionality ranged from 2 to 6 and was higher for the pre-odorant period compared to the odorant or reinforcement periods (GLM $p<0.01$, 18 d.f.). This indicates that Ca^{2+} ensemble activity becomes more uniform after addition of the odorant.

The identity of the stimulus can be decoded from MLI activity after mice learn to differentiate odorants. The finding that the MLIs developed divergent responses for S+ vs. S- trials following learning raised the question whether ensemble neural activity encodes for the identity of the stimulus when the animal becomes proficient differentiating the odorants. The learning curve for a session where the mouse achieves >80% ~60 trials is shown in Fig. 3a. Fig. 3b shows for this session plots of the first two principal components for a principal component analysis (PCA) of ΔF/F values for all MLIs for a subset of trials with percent correct <65% (top, naïve) or >80% (bottom, proficient) calculated for 1 sec before odorant application (pre-odorant), in the last second during odorant application (odorant) and for 1 sec after reinforcement (reinforcement, red: S+,

blue: S-). When the animal was naïve the S+ and S- data points appear to be spatially segregated for the reinforcement period, while for the proficient animal S+ and S- are segregated for both the odorant and reinforcement periods. This suggested that odorant identity (S+ vs. S-) could be decoded from ΔF/F values for proficient mice.

We utilized a linear discriminant analysis (LDA) to determine whether a hyperplane placed in the multidimensional space of ΔF/F values for all MLIs in the ensemble could decode the stimulus (S+ vs. S-). The LDA was trained with ΔF/F for all trials minus one and was queried to identify the odorant in the remaining trial (see Methods). The bootstrapped 95% confidence interval (CI) for an LDA trained after shuffling stimulus (S+ or S-) was used as a control. The time course for LDA decoding accuracy for the session with the learning curve in Fig. 3a is shown in Fig. 3c. For trials with percent correct <65%, decoding accuracy raises above the 95% CI after water reinforcement (Fig. 3ci), while in proficient trials, decoding accuracy starts rising above CI after odorant addition (Fig. 3cii). Fig. 3d shows a comparison of LDA decoding accuracy for the odorant and reinforcement periods vs. shuffled LDA for four mice. A GLM analysis yielded statistically significant interactions between (shuffled vs. odorant) x (proficient vs. naïve) and (shuffled vs. reinforcement) x (proficient vs. naïve) (GLM p values <0.01 and <0.05, 24 observations, 18 d.f.). Post hoc tests corrected for multiple comparison using false discovery rate (FDR)[28] yielded a statistically significant difference for decoding accuracy for either reinforcement or odorant vs. shuffled for proficient ($p<pFDR=0.007$, $n=4$). The data revealed that the accuracy for decoding the odorant identity from ΔF/F during the odorant period increases as the animal learns to differentiate between odorants.

MLI odorant responses switch when stimulus valence is reversed. In order to determine whether the MLIs responded to the chemical identity of the odorant, as opposed to responding to the valence (contextual identity: is the odorant rewarded?), we reversed odorant reinforcement. Fig. 4a shows an example of the learning curve for this reversal task. The animal reached proficiency in the initial training by learning to lick to 1% Iso (S+, forward period) and refrained from licking to odorless mineral oil (MO, S-, forward). When the rewarded odorant was switched the animal kept licking for Iso (now the S-), and percent correct dropped below 20%. As learning progressed, the animal gradually adjusted licking and successfully achieved the proficient level by licking for MO (S+) and not for Iso (S-). We analyzed how odorant-elicited changes in MLI ΔF/F varied in this reversal task. Fig. 4b shows single trial examples for mean ΔF/F odorant responses when the reward is reversed. MLIs respond to Iso (S+) with an increase in ΔF/F before reversal (forward trials 51 and 52), maintain the odorant increase in ΔF/F to what is now the unrewarded odorant (Iso, S-) immediately following reversal (reverse trials 91 and 92) and switch responses with increases to the new rewarded stimulus (MO, S+) when they become proficient in the reversal task (reverse trials 438 and 439). Fig. 4c shows for each trial the development of this reversal in MLI responses for this learning session. We found that the odorant-induced changes in ΔF/F for forward Hits (red circles) are substantial increases in ΔF/F that were maintained for ~20 trials after reversal (FAs, magenta). As the animal learned, the animal refrained to lick for Iso (S-, FAs became CRs, blue circles) and the odorant-induced changes in ΔF/F became small while the Missed trials (cyan) for MO became Hits with odorant-induced increases in ΔF/F. Fig. 4d shows the odorant-induced

ΔF/F changes for the forward and reverse periods for three mice when the animals were proficient (>80% correct). GLM analysis indicates that there is a significant difference in odorant-induced changes in ΔF/F for the odorant and the reversal ($p<0.001$, 12 observations, 8 d.f.). This example shows that after successful reversal the ΔF/F time course switched for the two odorants: the stimulus-induced increase in ΔF/F took place for the reinforced odorant, not for the chemical identity of the odorant.

Next we computed the accuracy for decoding the reinforced odorant for trials when the animal was proficient in either the forward or reverse trials using LDA analysis. Fig. 4e shows the time course for decoding accuracy for proficient trials in the forward (Fig. 4ei) and reverse (Fig. 4eii) periods for the reversal task in Fig. 4a. In both forward and reverse trials decoding accuracy rises above the 95% CI calculated with shuffled trials shortly after odorant addition. Finally, Fig. 4f shows the results of the forward and reverse LDA analysis for three mice that are proficient. GLM analysis indicates that differences in decoding accuracy are statistically significant between original and shuffled ($P<0.001$), but not between forward and reverse ($p>0.05$, $n=12$, 8 d.f.). These results indicate that for the proficient mouse it is possible to decode accurately contextual identity.

Accuracy for decoding the valence of the odorant from the activity of the MLI ensemble is highly variable for false alarms. To gain a better understanding of the information on odorant valence present in the responses of the MLI ensemble we asked whether stimulus decoding accuracy calculated with LDA for proficient mice differed between correct (Hits and CRs), and incorrect trials (Miss and FAs). If information in MLI

activity reflects the outcome of the trial we would expect that decoding accuracy would be lower for incorrect trials. On the other hand, if information in MLI activity reflects the stimulus regardless of trial outcome decoding accuracy would not differ between correct and incorrect trials. Fig. 5a shows the mean ΔF/F time courses (±CI) for each trial outcome for a proficient mouse performing the go-no go task. In this example Hits and Misses and CRs and FAs display similar time courses. Fig. 5b shows the spatial distribution of the first two principal components for each score during the last second of odorant exposure and the first second after reinforcement. The data show that S+ and S- responses are separate in PC space and that points for Miss and FA are mixed with Hit and CR trials respectively, suggesting that for this session decoding accuracy would be similar when evaluated separately for each trial outcome. To survey the information encoded in MLI activity in trials within different outcomes we utilized LDA analysis to decode the stimulus. Fig. 5c shows decoding accuracy for the odorant and reinforcement periods for the different trial outcomes and for shuffled data for six sessions. Decoding accuracy differed from shuffled for all outcomes and time periods (t test, $p<pFDR$, n=6 sessions, pFDR=0.025 for odorant and 0.0.25 for reinforcement). In addition, GLM did not yield a significant difference for outcomes (Hit, Miss, CR or FA) or time period (odorant vs. reinforcement) (48 observations, 40 d.f. $p>0.05$). However, we noticed that decoding accuracy displayed a large variance for FA. Indeed, a two-sample *F*-test for equal variances indicated that the variance differs between FA and CR ($p<pFDR=0.025$, n=6). This analysis determined that odorant-induced MLI Ca^{2+} changes carries information on the stimulus, as opposed to the outcome, but that the variance for the accuracy of stimulus decoding is significantly higher for FA compared to CR.

Changes in lick rate correlate with changes in MLI activity during reinforcement, but not during odorant application. Sustained dry licking is the motor output that results in release of water reward for the go-no go task. Lick rate is encoded by MLI activity in Crus II[29,30]. To explore whether the observed MLI ensemble activity we recorded in vermis is directly related to licking we examined the lick pattern for S+ and S- trials and the correlation between the derivative of the ΔF/F time course and the derivative of the lick rate[29]. Records of licks for S+ and S- trials for a typical go-no go session are shown in Fig. 6a. In the learning period (percent correct <65%, Fig. 6a,i), the animal failed to lick for a subset of trials during the 4 second odorant exposure period in S+ trials (Miss trials). In contrast, when the animal was proficient (>80% correct, Fig. 6a,ii, right) the animal learned to sustain licking for the two 2 sec segments during application of the S+ odorants, increased licking after receiving the water reward and refrained from licking for the S- trials. Fig. 6b shows the lick frequency for this example and Fig. 6c shows the p value calculated with a ranksum test comparing licking between S+ and S- trials. For the proficient mouse the lick frequency diverges between S+ and S- trials shortly after addition of the odorant (Fig. 6b,ii) and this divergence is evidenced by a large decrease in the p value below 0.05 (Fig. 6c,ii).

In order to explore the relationship of MLI activity to licking we proceeded to calculate the correlation between the derivative of the ΔF/F time course (D_tMLI-F) and the derivative of the lick rate (D_tLR)[29]. Fig. 6d shows examples for several trial outcomes for the time course for ΔF/F and the lick rate. We computed the derivative of these two parameters and plotted

their relationship during different time periods for the proficient mouse. Fig. 6e shows an example of this relationship for a go-no go session. The correlation between the derivative of the ΔF/F time course and the derivative of the lick rate is significant for the reinforcement period (ρ=0.37, $p<0.001$), and is smaller for both the pre-odorant and odorant periods (ρ=-0.045 and -0.12, $p>0.05$). Fig. 6f shows the average (±CI) of the correlation coefficients calculated for six sessions. As found in Crus II, the D_tMLI-F and D_tLR are positively correlated during the reward period. In contrast, these two variables display much lower correlations during the pre-odorant and odorant periods. A t test corrected for multiple comparisons indicated that there is a statistically significant difference in the correlation coefficient between the reinforced and odorant periods ($p<pFDR=0.017$, n=6). These data suggest that changes in ΔF/F for MLI activity during the odorant application period do not reflect changes in lick activity.

The main contributor during the period of odorant application to a fit of a GLM model to MLI activity is the contextual identity of the odorant. In order to understand the contribution of different behavioral and stimulus variables to MLI activity we setup a GLM to quantify the dependence of the average ΔF/F on the different behavioral and stimulus variables[31]. We included "event" variables, "whole trial" variables and "continuous" variables (Fig. 7a, Methods). Continuous variables quantified kinematics including lick rate, the derivative of lick rate and the velocity and acceleration of movements made by the head fixed animal during the trial. The identity of the odorant (S+/S- odorant) was an event variable that increased from zero to one during the time for S+ or S- odorant application. Finally, whole trial variables were accuracy (1 for correct and

0 for incorrect responses), reinforcement history (1 for reinforcement in the last trial, 0 otherwise) and percent correct behavior calculated in a window of 20 trials.

Black traces in Fig. 7b show examples of the fit of the GLM model to average ΔF/F time courses for four example trials with different outcomes. The fit traces in black largely overlap with the recorded data. When quantified over the different periods within a trial (pre-odorant, odorant and reinforcement) we found that the GLM explained a substantial percent of the average ΔF/F variance ranging from 23.5% to 95% (Fig. 7c). We next quantified the relative contribution of the different variables to the ensemble activity in the three time periods. Fig. 7d shows the contributions to the GLM fit by the variables that make the largest percent contribution to the fit (kinematics, licks, reinforcement history and odorants). Odorant (S+ vs. S-) is the dominant contributor to the activity during odorant application (Fig. 7d,iii, asterisks show differences with ranksum or t test $p<pFDR=0.033$, $n=6$). Furthermore, variables describing the licks contribute to the GLM fit during the outcome period (Fig. 7d,ii, * $p<pFDR=0.016$ for a t test, $n=6$). In contrast, the other two variables (kinematics and reinforcement history) do not differ in contribution during the different periods ($p>pFDR=0.017$, ranksum test). These data indicate that odorant identity contributes to prediction of MLI activity during the odorant application period while licks contribute to MLI activity during the reinforcement period.

Chemogenetic inhibition of MLI activity leads to impaired go-no go learning. In order to determine whether activity of MLIs plays a role in behavioral responses in the go-no go task we used a Cre-dependent AAV virus to express the inhibitory DREADDs receptor

hM4Di in MLIs in six PV-Cre mice (hM4Di group)[23]. To control for off-target effects of clozapine-N-oxide (CNO)[32] we injected PV-Cre mice with Cre-dependent mCherry AAV virus in another group of six mice (mCherry group). One to two weeks later animals from both groups were trained to differentiate two odorant mixtures (S+: 0.1% of 60% heptanal+40% ethyl butyrate, S-: 0.1% of 40% heptanal+60% ethyl butyrate) for 3-4 sessions encompassing 400-500 trials in the go-no go task. For these sessions the animals were injected intraperitoneally (IP) with saline 40 minutes before the start of the sessions (mCherry-saline and hM4Di-saline). One to two weeks later mice were trained again to differentiate between the same odorant mixtures, but they were injected IP with CNO (3mg/kg) 40 minutes before the start of the session (mCherry-CNO and hM4Di-CNO).

Figs. 8a,i and b,i show representative examples of the behavioral performance for the four conditions. Mice in all groups with the exception of the hM4Di-CNO attained proficiency (>80% percent correct). The bar graphs in Figs. 8a,ii and b,ii show the average percent correct for all trials ($\pm$CI, n=6 mice per condition). GLM analysis indicates that there is a statistically significant interaction between CNO drug treatment and hM4Di expression ($p<0.01$, 24 observations, 20 d.f.) and post hoc tests corrected for multiple comparisons indicate that the h4DMi expressing group differs between CNO and saline ($p<pFDR=0.025$, n=6 mice per group), while there are no significant differences between CNO and saline for the mice expressing mCherry ($p>pFDR$, n=6 mice per group), indicating an effect of CNO-induced inhibition of MLIs expressing h4DMi on behavioral output and the absence of off-target CNO effects.

We proceeded to compare the time course for lick frequency between different conditions for trials when the mouse was proficient (>80% correct, Fig. 8c). Interestingly, the divergence in lick frequency between S+ and S-, that takes place shortly after odorant addition for mCherry mice (±CNO) and for h4DMi mice injected with saline, is slower for h4DMi mice injected with CNO (inset in Fig. 8c,ii). This is likely why the h4DMi mice injected with CNO accumulated errors in the go-no go task shown in Fig. 8b. In order to quantify this difference in lick frequency we calculated the lick frequency shortly after odorant addition (0.8 to 1.8 seconds after odorant addition, Fig. 8d). For S+ (Fig. 8di) GLM analysis did not find a statistically significant difference for treatment or h4DMi expression (or interactions) for the rewarded odorant trials ($p>0.05$, 53 observations, 49 d.f.), but GLM did find a statistically significant difference for S- (Fig. 8dii) for the interaction between CNO treatment and h4DMi expression ($p<0.001$, 53 observations, 49 d.f). These data suggest that inhibition of MLIs in vermis causes a slower differential lick response to the odorants leading to impaired behavioral performance.

Discussion

We found that vermal MLIs developed a differential response to odorants in the go-no go task and that the response switched when the valence of the odorants was reversed. Decoding analysis revealed that when the animal was proficient the contextual identity of the odorant (is this stimulus rewarded?) could be predicted from MLI responses shortly after addition of the stimulus. GLM analysis revealed that contextual identity made a large contribution to predicting the changes in Ca^{2+} in the MLIs during the odorant application period. Chemogenetic inhibition of MLIs impaired achievement of proficient discrimination of odorants. These data indicate that processing by MLIs plays a role in associative learning.

The cerebellum has been widely implicated in mediating supervised learning through an iterative process whereby the system's response to a given input is evaluated against a desired outcome, and errors are then used to adjust adaptive elements within the system[8-10,33]. CFs carrying error signals make profuse synaptic connections on the dendrites of PCs and CF stimulation elicits powerful excitatory dendritic Ca^{2+} spikelets[34-36]. Furthermore, recent studies indicate that CFs also signal reward prediction[11,12] or decision-making errors[13], and the cerebellum modulates association pathways in VTA enabling a cerebellar contribution to reward-based learning and social behavior[14]. The increase in Ca^{2+} mediates LTD in subsets of synapses innervated by co-activated granule cell parallel fibers (PFs) carrying sensorimotor information relevant to learning[37,38]. Because of the reliability of CF fiber-elicited dendritic Ca^{2+} changes and plasticity this learning process was proposed to

be “all or none”[39]. However, recent studies by Rowan et al.[18] revealed that increasing feed forward inhibition by MLIs can switch the valence of plasticity from LTD to LTP (also, see[40]). In addition, adaptive changes in the vestibulo-ocular reflex elicited by CF optogenetic activation switched from increase to decrease depending on whether MLIs were co-activated using optogenetics[18]. Finally, MLIs gate supralinear CF-evoked Ca2+ signaling in the PC dendrite[41]. These studies suggest that the valence of learning is graded by MLI activity.

Here we provide evidence for the involvement of MLIs in conveying information on contextual identity of a stimulus in associative learning. A question that arises is which circuit mechanism is responsible for mediating the switch in MLI responsiveness when odorant valence is reversed. MLIs receive sensorimotor information from multiple GCs through PF input and *in vivo* studies have found remodeling of MLI receptive fields upon repeated electrical stimulation of the skin[42]. In addition, plasticity in PF-MLI synapses are postulated to increase the information capacity of the MLI-PC network and richness of PC output dynamics[10,43], and a model of PF-MLI plasticity has been proposed[44]. If long term plasticity of PF-MLI synapses is indeed responsible for the large change of MLI responsiveness found here upon reversal of stimulus valence it is likely that the error signal would be provided by CF spillover[45]. However, the switch in MLI responsiveness could also be due to changes in GC activity. Indeed, recent studies of GC responsiveness have shown that GCs encode for reward anticipation in an operant conditioning task[25] and that they acquire a widespread predictive feedback in motor learning[24]. Finally, we found that

inhibition of MLIs by DREADDs slowed decision-making, consistent with a role for the CF/PC circuit in reward timing prediction[46].

Interestingly, odorant responses have been reported in the cerebellum in rodents and humans. Studies of c-Fos expression found that when sexually trained male rats were exposed to female bedding or almond smell they displayed higher levels of cFos immunoreactive GCs in the vermis compared to rats exposed to clean air[47]. In addition, sexual experience increased the number of cFos positive GCs. In humans odorants induced significant activation of the cerebellum in an fMRI study[48]. In addition, human cerebellar lesions caused olfactory impairments in the contralesional nostril, and elicited sniffs with lower overall airflow velocity and volume in comparison with controls[49]. The authors concluded that the findings implicate an olfactocerebellar pathway prominent in odorant identification and detection that functionally connects each nostril primarily to the contralateral cerebellum. Our study provides further evidence for involvement of the cerebellum in olfactory sensorimotor tasks.

Our findings show that differential MLI activity develops during learning in an associative learning task and that MLI activity switches when the rewarded odorant is reversed. We find that inhibition of MLI activity elicits decreased behavioral performance in the go-no go task. Our data indicate that MLIs have a role in learning valence. This would likely increase the information capacity of the MLI-PC network and richness of PC output dynamics[10,43].

Acknowledgments: We thank Ms. Nicole Arevalo for animal husbandry, Ms. Dnate' Baxter for laboratory support, Ms. Arianna Gentile-Polese for help with the summary figure and Mr. Jesse Gilmer with help coding dimensionality. We thank Mr. Matt I. Becker, Mr. Jesse Gilmer, Dr. Isabel Llano and Dr. Abigail Person for discussions. This research was supported by NIDCD 5R01DC000566, NINDS U01 NS099577 and NSF CBET-1631912.

Author contributions: M.M., and D.R. designed all experiments aided with discussions with E.G., B.O. and G.F., while M.M. G.F. and D.R. performed them. E.G., G.F. and B.O. designed, setup and maintained the custom two-photon microscope, M.M. and D.R. set up the olfactometer. D.R. wrote all programs for data collection and analysis. M.M. and D.R. analyzed the data. M.M. and D.R. generated the figures. All authors discussed the results. M.M. and D.R. wrote the manuscript, and all authors participated in commentary and revision of the manuscript.

Declaration of interests: The authors declare no competing interests.

Methods

Animals

All animal procedures were performed in accordance with protocols approved by the Institutional Animal Care and Use Committee of the University of Colorado Anschutz Medical Campus. Mice were bred in the animal facility. We used both male and female adult Parvalbumin-Cre (PV-Cre, Jackson Labs stock number 008069) mice and wild-type C57BL/6J mice. The animals were housed in a vivarium with a 14/10h light/dark cycle. Food was available ad libitum. Access to water was restricted in for the behavioral training sessions according to approved protocols, all mice were weighed daily and received sufficient water during behavioral training to maintain >80% of original body weight.

Immunohistochemistry

To perform immunostaining, mice were sacrificed and transcardially perfused with ice cold 4% PFA, followed by incubation in 30% sucrose. After the brain sank in the sucrose solution 60 μm thick slices were cut with a cryostat. The slices were imaged using a confocal laser scanning microscope (Leica TCS SP5II or Nikon A1R) to determine the GCaMP expression patterns in the cerebellum. The slices were counterstained with DAPI.

Window Implantation

Adult mice (8 weeks or older) were first exposed to isoflurane (2.5%) and then maintained anesthetized by intraperitoneal ketamine-xylazine injection (100 μg/g and 20 μg/g). A craniotomy was made over the vermis of cerebellum centered at midline 6.8 mm posterior to Bregma leaving the dura intact (lobule VI). A square glass window (2 mm x 2 mm) was

placed over the craniotomy and the edges were sealed with cyanoacrylate glue (3M, USA). The window was further secured with Metabond (Parkell, USA), and a custom-made steel head bracket was glued to the skull.

Virus Expression of GCaMP

In order to express GCaMP6f in cerebellar MLIs we injected the vermis of the cerebellum in three adult PV-Cre mice with 2.0 μl of AAV1-Syn-Flex-GCaMP6f (Addgene, USA) (6.8 mm posterior to Bregma, bilaterally ±0.5 mm lateral to midline and 200-400 μm below the brain surface)[22]. The viral infection method we use has been reported to express GCaMP in MLIs, and not in PCs[50,51]. Supplementary Fig. 2 shows that indeed expression of GCaMP6 takes place only in MLIs. Expression in MLIs may reflect the differential activity of the hSyn promoter, and has been described for a different genetically-encoded Ca^{2+} indicator[51]. In one C57BL/6 animal each we used AAV5-Syn-GCaMP6s or AAVrg-Syn-jGCaMP7f (Addgene, USA) with similar results to those obtained with GCaMP6f and therefore the data were pooled. After the injection, the animals were maintained for at least three weeks before behavior training and imaging.

Go-No Go Training

Mice were water deprived by restricting daily consumption of water to 1-1.5 ml. Mice were monitored for signs of dehydration or a decrease in body weight below 80% of the initial weight. If either condition occurred the animals received water ad-lib until they recovered. When the animals were ready, they were trained in a head-fixed olfactory go-no go task with (1% iso-amyl acetate vs mineral oil odorant application)[19,52]. Licks were monitored

by an olfactometer that controlled valves to deliver a 1:40 dilution of odorant at a rate of 2 lt/min. The water-deprived mice started the trial by licking on the water port. In S+ trials, the mice needed to lick at least once in two 2 sec time periods to obtain a reward (0.1 g/ml sucrose water). In S- trials, the mice need to refrain licking one of the two 2 sec segments to avoid a longer inter-trial interval (10 sec). The animal's behavior performance was evaluated in a sliding window of 20 trials (10 for S+ and S- trials each, presented in random order). The percent correct value represents the percent of trials in which the animal successfully performed appropriate actions, and we considered the animal proficient if percent correct performance is above 80%. In reverse go-no go training sessions, the rewarded and un-rewarded odorants were switched. Movement of the mouse was imaged in the infrared to prevent light interference with the non-descanned detection in the visible using a 1 Megapixel NIR security camera (ELP-USB100W05MT-DL36, Amazon.com) at 30 frames per second. Velocity of body movement was estimated using the Farneback algorithm coded in Matlab[53].

Behavioral performance recorded after chemogenetic inhibition of MLI activity

For chemogenetic inhibition of MLI activity[23,32], 1.2 ul of AAV8-hSyn-DIO-hM4D(Gi)-mCherry virus (Addgene, USA) were bilaterally injected into 6 PV-Cre animals bilaterally ±0.5 mm lateral to midline, 6.8 mm posterior to Bregma and 200-400 μm below the brain surface. For control an AAV8-hSyn-DIO-mCherry virus (Addgene, USA) was injected in the same position in 6 PV-Cre animals. This viral infection method results in expression of the protein in MLIs, and not in PCs[50,51]. Four weeks after injection the animals were trained to proficiency in the go-no go task with 0.1% iso-amyl acetate (S+) vs MO (S-). When they

reached a proficient level, the animals rested for one to two weeks, and were then injected intraperitoneally (IP) with saline 40 minutes before starting the session and were trained to discriminate between two odorant mixtures: 0.1% of 60% heptanal+40% ethyl butyrate (S+) and 0.1% of 40% heptanal+60% ethyl butyrate (S-) for 3-4 sessions for a total of 400-50 trials. The animals then rested for one to two weeks and were subsequently trained to discriminate the same odorant mixtures in sessions that took place 40 minutes after IP injection of 3mg/kg clozapine-N-oxide.

Two Photon Imaging of MLI Activity in Animals Undergoing the Go-No Go Task

All the animals were first habituated to the setup to minimize stress during the imaging experiments. All the imaging sessions started at least 10 minutes after mice had been head-fixed. We searched for active MLIs while imaging zones in the vermis of lobule VI, between the midline and the paravermal vein, an area of the cerebellum where GCs acquire a predictive feedback signal or expectation reward[24,25]. The head fixed two photon imaging system consisted of a movable objective microscope (MOM, Sutter Inc) paired with a 80 MHz, ~100 femtosecond laser (Mai-Tai DeepSee, Spectra Physics, USA) centered at 920 nm. The MOM was fitted with a single photon epifluorescence eGFP filter path (475 nm excitation/500-550 nm emission) used for initial field targeting followed by switching to the two photon laser scanning path for imaging GCaMP at the depth of the MLIs. The galvometric laser scanning system was driven by SlideBook 6.0 (Intelligent Imaging Innovations, Inc). The two photon time lapses were acquired at 256 x 256 pixels using a 1.0 NA/20x water emersion objective (Zeiss, Germany) at 5.3 Hz. On the day of initial imaging, a field of view was selected to image a large number of active cerebellar neurons

located in the most superficial planes of the molecular layer likely including mostly stellate cells, and several batches of 6000 frames were be collected in each training session. After two photon imaging a second image of the vasculature was captured wide field epifluorescence to reconfirm the field.

Data Analysis

Raw imaging data was first surveyed in Image J to exclude image sequences exhibiting axial movement. We did not find evidence of axial movement while the animal was engaged in the go-no go task. In addition, we performed control imaging where we excited GCaMP6f at 820 nm, a two photon excitation wavelength where fluorescence emission is Ca^{2+}-independent[54]. Supplementary Fig. 5 shows that we did not detect transient changes in GCaMP6 fluorescence in a mouse engaged in the go-no go task when the cells were excited at 820 nm. If we found horizontal drift due to motion, we applied cross correlation-based image alignment using the Turboreg, Image J plugin. The data were then analyzed with CaImAn Matlab software that uses constrained nonnegative matrix factorization to define independent spatial and temporal components corresponding to changes in GCaMP fluorescence in individual MLIs[26]. Baseline of intensity ($F0$) was defined as the mean fluorescence intensity before trial start, defined as the time when the animal first licked. This was when fluorescence started to increase above baseline and the odorant was added at a random time 1-1.5 seconds after trial start. Intensity traces (F) were normalized according to the formula $\Delta F/F = (F - F0)/F0$. After CaImAn analysis, the $\Delta F/F$ traces of the spatial components were sorted and we assigned trial traces to different

behavioral events (Hit, CR, Miss and CR) and aligned them to trial start, odorant onset or water delivery.

Statistical Analysis

Statistical analysis was performed in Matlab. Statistical significance for changes in measured parameters for factors such as learning and odorant identity (S+ vs. S-) was estimated using a generalized linear model (GLM), with post-hoc tests for all data pairs corrected for multiple comparisons using false discovery rate[28]. The post hoc comparisons between pairs of data were performed either with a t-test, or a ranksum test, depending on the result of an Anderson-Darling test of normality. 95% confidence intervals (CIs) shown in the figures as vertical black lines or shading bounding the lines were estimated by bootstrap analysis of the mean by sampling with replacement 1000 times.

Principal component analysis was calculated using the Matlab Statistics Toolbox. Classification of trials using $\Delta F/F$ measured from all components in the field of view was accomplished via linear discriminant analysis (LDA) in Matlab. $\Delta F/F$ for all components for every trial except one were used to train the LDA, and the missing trial was classified by its fit into the pre-existing dataset. This was repeated for all trials and was performed separately for analysis where the identity of the odorants was shuffled. Fluorescence intensity traces, lick rates and kinematics in Fig. 7 were low-pass filtered with a hamming window of a time constant of 0.59 s.

Dimensionality

Following Litwin-Kumar et al.[55] we defined the dimension of the system (dim) with *M* inputs as the square of the sum of the eigenvalues of the covariance matrix of the measured ΔF/F for all ROIs in the FOV divided by the sum of each eigenvalue squared:

$$\dim(\Delta F/F) = \left(\sum_{i=1}^{M} \lambda_i\right)^2 / \left(\sum_{i=1}^{M} {\lambda_i}^2\right)$$

where λ_i are the eigenvalues of the covariance matrix of ΔF/F computed over the distribution of ΔF/F signals measured in the FOV. If the components of ΔF/F are independent and have the same variance, all the eigenvalues are equal and dim(ΔF/F) = *M*. Conversely, if the ΔF/F components are correlated so that the data points are distributed equally in each dimension of an *m*-dimensional subspace of the full *M*-dimensional space, only *m* eigenvalues will be nonzero and dim(ΔF/F) = *m*.

Generalized Linear Modelling Estimate of Contribution of Different Variables to Changes in ΔF/F

In order to quantify the contribution of different variables to neural activity, we used GLM as described by Engelhard et al. [31]. We used the Matlab fitglm function to fit the per trial ΔF/F time course for mice proficient in the go-no go task with a GLM. We included "event" variables, "whole trial" variables and "continuous" variables. Continuous variables quantified kinematics including lick rate, the derivative of lick rate and the velocity and acceleration of movements made by the head fixed animal during the trial. The identity of the odorant (S+/S- odorant) was an event variable that increased from zero to one during the time for S+ or S- odorant application. Finally, whole trial variables were accuracy (1

for correct responses and 0 for incorrect responses), reinforcement history (1 for reinforcement in the last trial, 0 otherwise) and percent correct behavior calculated in a window of 20 trials.

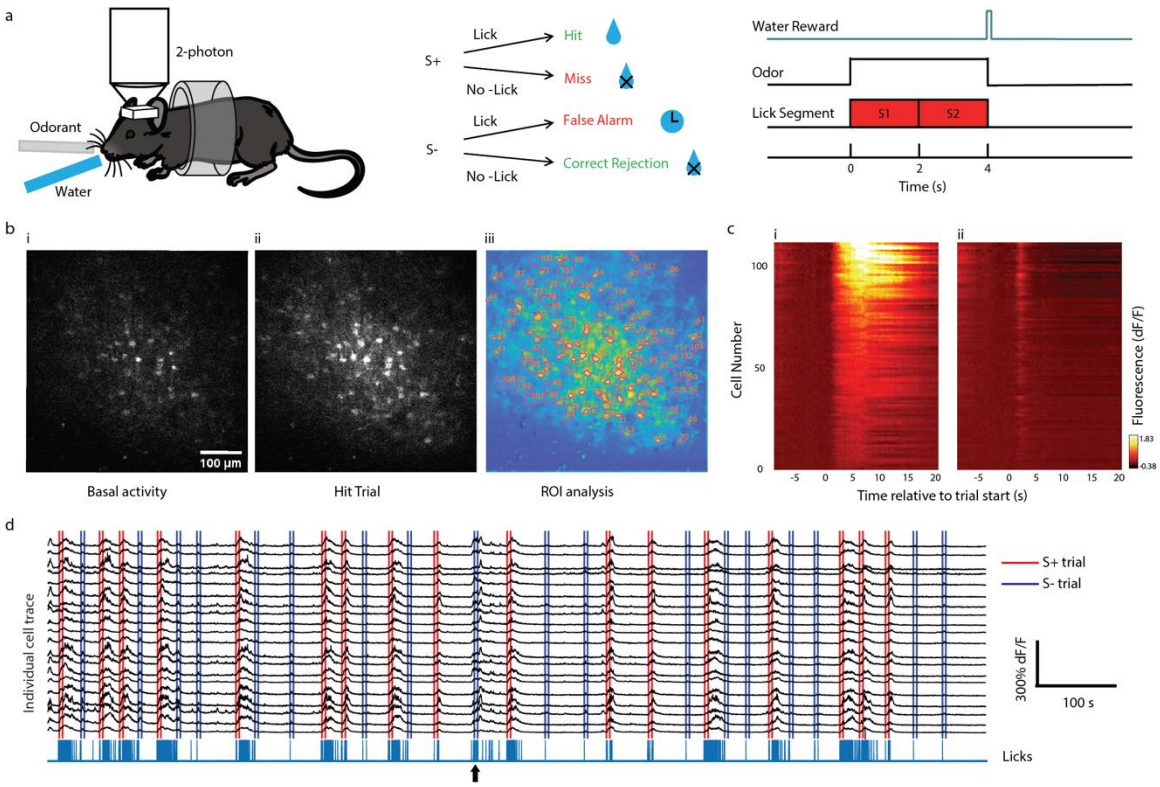

Figure 1. Two-photon Ca^{2+} imaging of MLIs in head-fixed mice undergoing the go-no go associative learning task.

a. Go-no go task. Left: Two-photon imaging of a head-fixed mouse responding to odorants by licking on a water spout in response to the rewarded odorant in the go-no go task. Center: Scoring of decision making. Right: time course of the trial. For water reward in Hit trials the animal must lick at least once in each of the two 2 second segments.

b. The panels in **i** and **ii** show two photon microscopy images of GCaMP6f fluorescence recorded in MLIs from a mouse proficient in the go-no go task (basal activity: before trial start, Hit trial: during reinforced odorant application). The color image in **iii** shows the components (regions of interest) identified using CaImAn software[26].

c. Pseudocolor plots displaying the average per trial ΔF/F time course for Hit (**i**) and CR (**ii**) odorants for all ROIs in this example.

d. Neural ensemble activity. Black traces are the GCaMP6f fluorescence (ΔF/F) time courses for a subset of the ROIs identified in the field of view in **b**. This mouse was proficient (>80% correct trials). Vertical lines: red start and end of S+ odorant application, blue is S-. The blue trace at the bottom shows the licks. All trials were Hits or CRs with the exception of the trial identified with the arrow that was a FA.

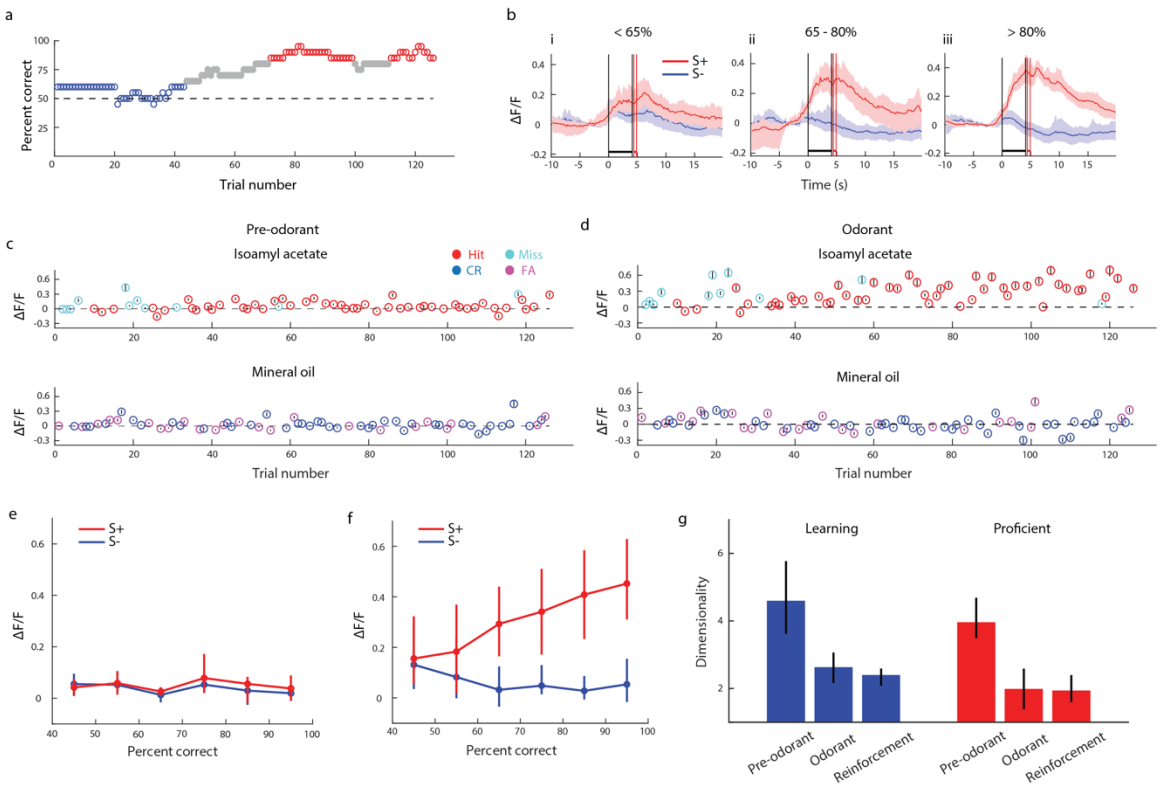

Figure 2. MLIs developed divergent responses during go-no go learning.

a. Learning curve for a mouse discriminating 1% isoamyl acetate from mineral oil in the go-no go task. Red dots: proficient level (>80% percent correct), blue dots: percent correct <65%.

b. GCaMP6f fluorescence (ΔF/F) time course averaged over all ROIs and trials falling within different proficiency windows. **i.** < 65%, **ii.** 65%-80% and **iii.** > 80%. (red: S+, blue: S-, the shaded area is the 95% confidence intervals). The vertical black lines are odorant onset and removal and the red lines bound the reinforcement period.

c-d. Per trial ΔF/F averaged over all ROIs for one second before odorant application (**c**, Pre-odorant**)** and in the last second of odorant application (**d,** Odorant). Vertical lines around the mean of each trial are the CI.

e-f. ΔF/F for four mice averaged over all the ROIs for all trials falling within different proficiency windows. ΔF/F average was calculated for one second before odorant application (**e**) and for the last second after odorant application (**f**). For the data during odorant application (**f**) a generalized linear model (GLM) analysis indicated that there is a statistical significance for the interaction between percent correct and the identity of the odorant ($p<0.001$, 44 d.f., data from 4 mice). GLM did not yield statistically significant differences for pre-odorant data (**e**, $p>0.05$, 44 d.f., data from 4 mice)**.**

g. Dimensionality for ΔF/F calculated in three periods: pre-odorant: 1 sec before odorant onset, odorant: last second of odorant application, reinforcement: 1 sec after the onset of water reward.

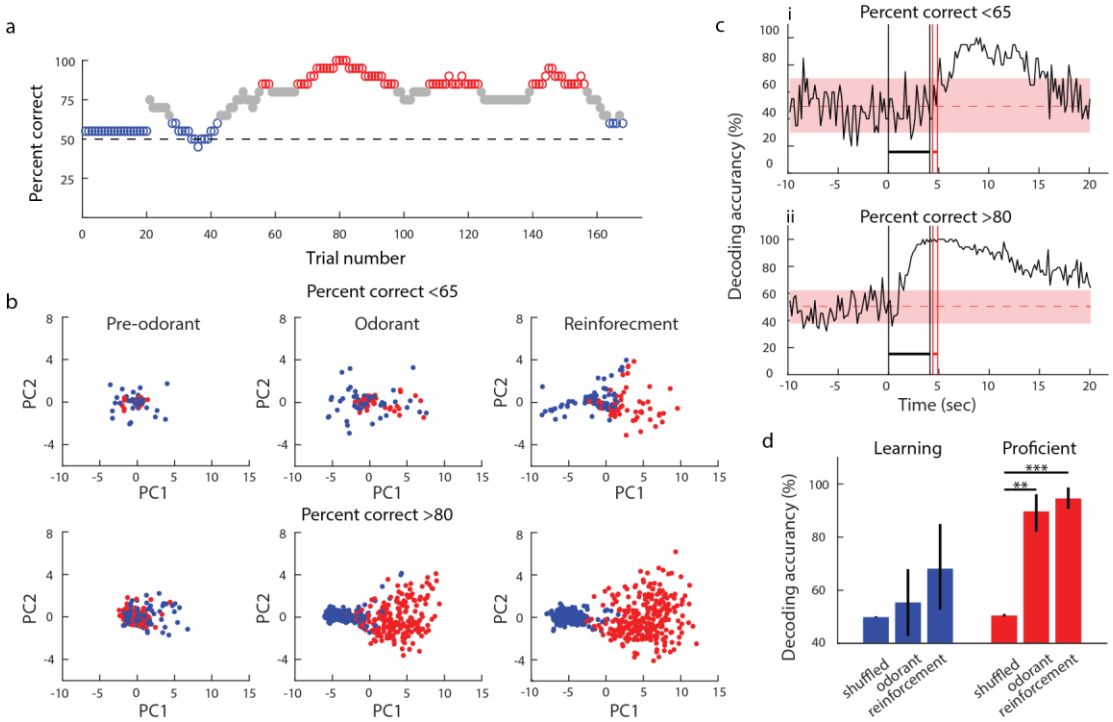

Figure 3. The accuracy of decoding the stimulus increases as the animal learns to discriminate the odorants.

a. Learning curve for a mouse performing the head-fixed go-no go task. Red dots: proficient level (>80% percent correct), blue dots: percent correct <65%.

b. First two principal components for the PCA for the changes in GCaMP6f fluorescence (ΔF/F) in all the ROIs in the FOV. Top: the mouse was performing < 65% correct, bottom: the same mouse was performing >80% correct. The principal components are shown for three time periods: Pre-odorant: 1 sec before odorant addition, odorant: 1 sec before removal of the odorant, and Reinforcement: 1 sec after reward. Red circles: S+ trials, blue circles: S- trials.

c. Decoding accuracy for the linear discriminant analysis (LDA) trained to predict odorant identity using ΔF/F for all ROIs in the FOV. Shade: 95% confidence interval for LDA

trained with shuffled odorant identity. The vertical black lines are odorant onset and removal and the red lines bound the reinforcement period.

d. LDA decoding accuracy calculated from the ($\Delta F/F$) for all ROIs in the FOV from data recoded in four mice. A GLM analysis of decoding accuracy yielded statistically significant interactions between (shuffled vs. odor) x (proficient vs. naïve) and for (shuffled vs. reinforcement) x (proficient vs. naïve) (GLM p values <0.01 and <0.05, 24 observations, 18 d.f.). The vertical lines show 95% CIs. The asterisks denote significant post hoc tests corrected for multiple comparison using false discovery rate (FDR, $p<pFDR=0.007$, $n=4$).

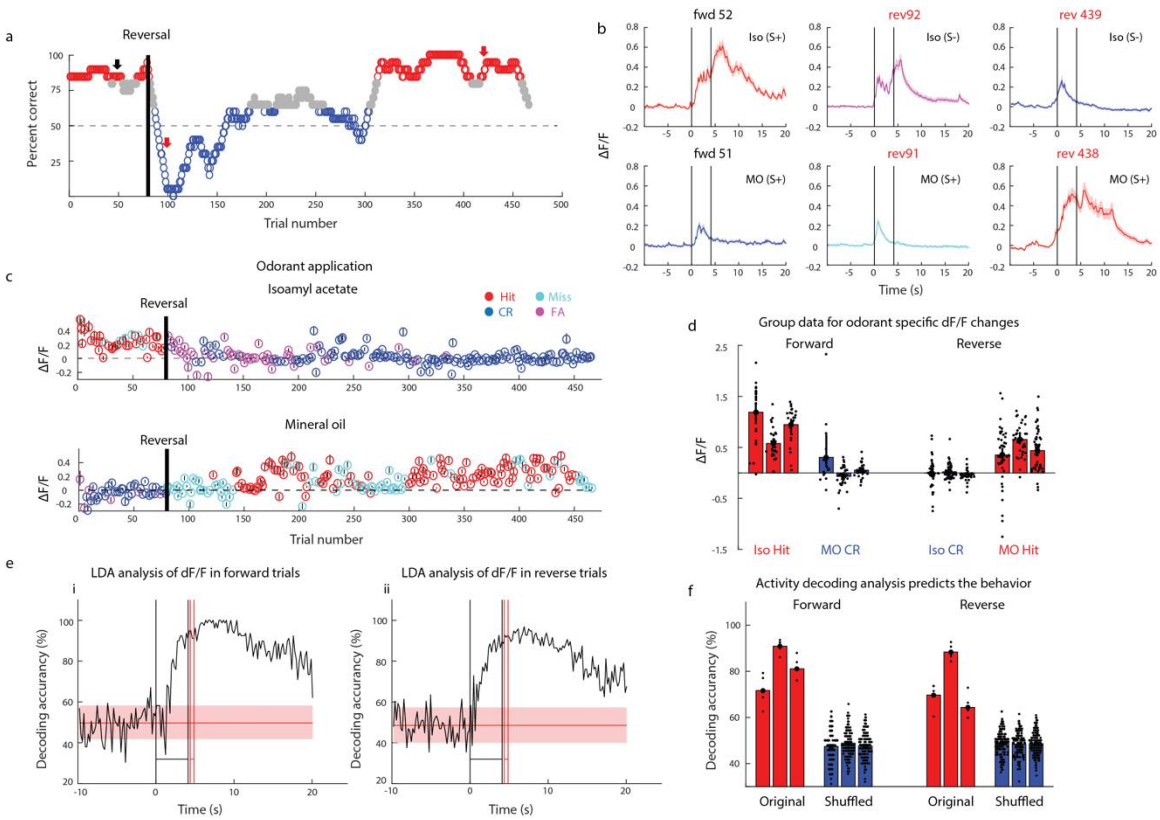

Figure 4. MLI odorant responses switched after reversal.

a. Learning curve showing the animal's behavior after reversal. Blue <=65%, red: >80% correct. Forward: S+ 1% isoamyl acetate (Iso) and S- mineral oil (MO).

b. Average ΔF/F time courses for example trials before (trials 51 and 52) and shortly after (trials 91 and 92) reversal, and after the animal attained proficiency after reversal (trials 438 and 439). The vertical black lines are odorant onset and removal.

c. Per trial average ΔF/F during the last second of odorant application for the reversal task in Fig. 4a. The upper plot shows the responses to Iso and the lower plot shows responses to MO.

d. Odorant-induced changes in ΔF/F recorded from three animals computed for trials when the animal was behaving >80% correct. Vertical lines are 95% CIs. Red: S+, Blue: S-. A

GLM analysis indicates that there is a significant difference in odor-induced changes in $\Delta F/F$ for both odorant and reversal ($p<0.001$, 12 observations, 8 d.f.).

e. Time course for decoding accuracy computed with LDA analysis of $\Delta F/F$ data for all ROIs in the FOV. The shade is the 95% confidence interval of decoding accuracy calculated with shuffled odorant identity. The vertical black lines are odorant onset and removal and the red lines bound the reinforcement period.

f. Decoding accuracy for three animals calculated with odorant-induced changes in $\Delta F/F$ from trials where the animal was performing >80% correct. Vertical lines are 95% CIs. Red: S+, Blue: S-. A GLM analysis indicates that differences in decoding accuracy are statistically significant between original and shuffled ($P<0.001$), but not between forward and reverse ($p>0.05$, $n=12$, 8 d.f.).

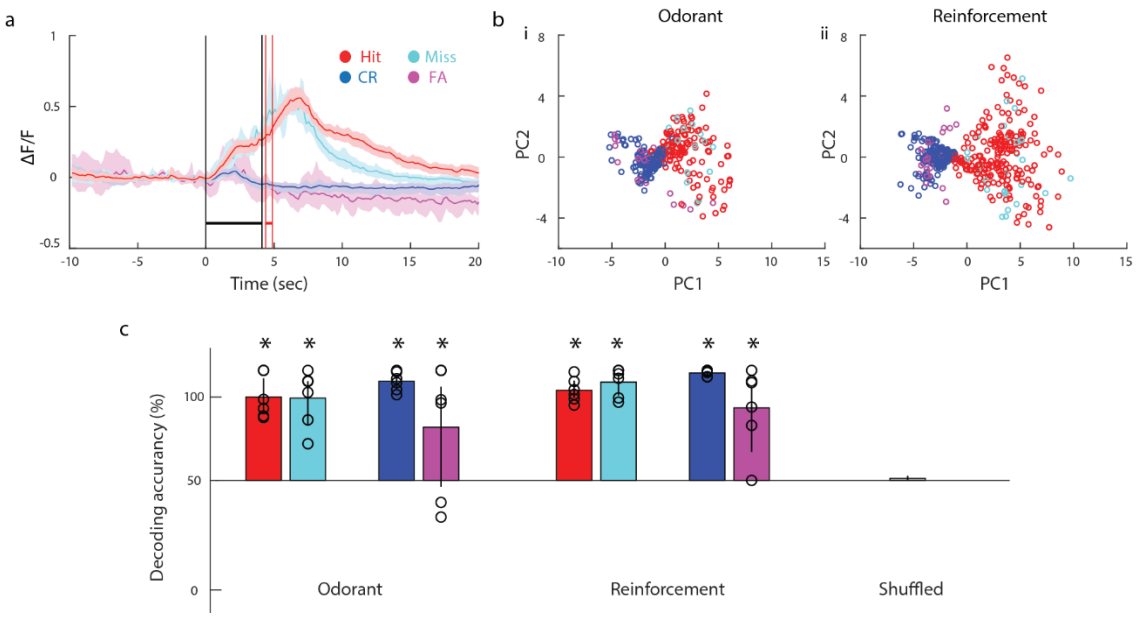

Figure 5. Discriminant analysis of stimulus prediction for error trials.

a. Time course for average ΔF/F (±CI, shade) for the four trial outcomes for a mouse performing at percent correct >80%. The color indicates the outcome of the trial (Red: Hit, Cyan: Miss, Blue: CR and Magenta: FA). The vertical black lines are odorant onset and removal and the red lines bound the reinforcement period.

b. Plots of the spatial arrangement of the first two principal components from a PCA analysis of ΔF/F for all ROIs in the FOV for the session shown in a. The time periods used for the PCA were the last second of the odorant application (**i**) and one second following reinforcement (**ii**).

d. Decoding accuracy for LDA analysis of stimulus prediction calculated with ΔF/F for all ROIs in the field of view classified by trial outcome. The LDA analysis was performed for five mice (six sessions, for one mouse two sessions were included). Decoding accuracy differed from shuffled for all outcomes and time periods (t test, p<pFDR=0.0125, n=6 sessions). GLM did not yield a significant difference for score categories or time period

(odorant vs. reinforcement) (48 observations, 40 d.f. $p>0.05$). A two-sample F-test for equal variances indicated that the variance differs between FA and CR ($p<pFDR$, $n=6$).

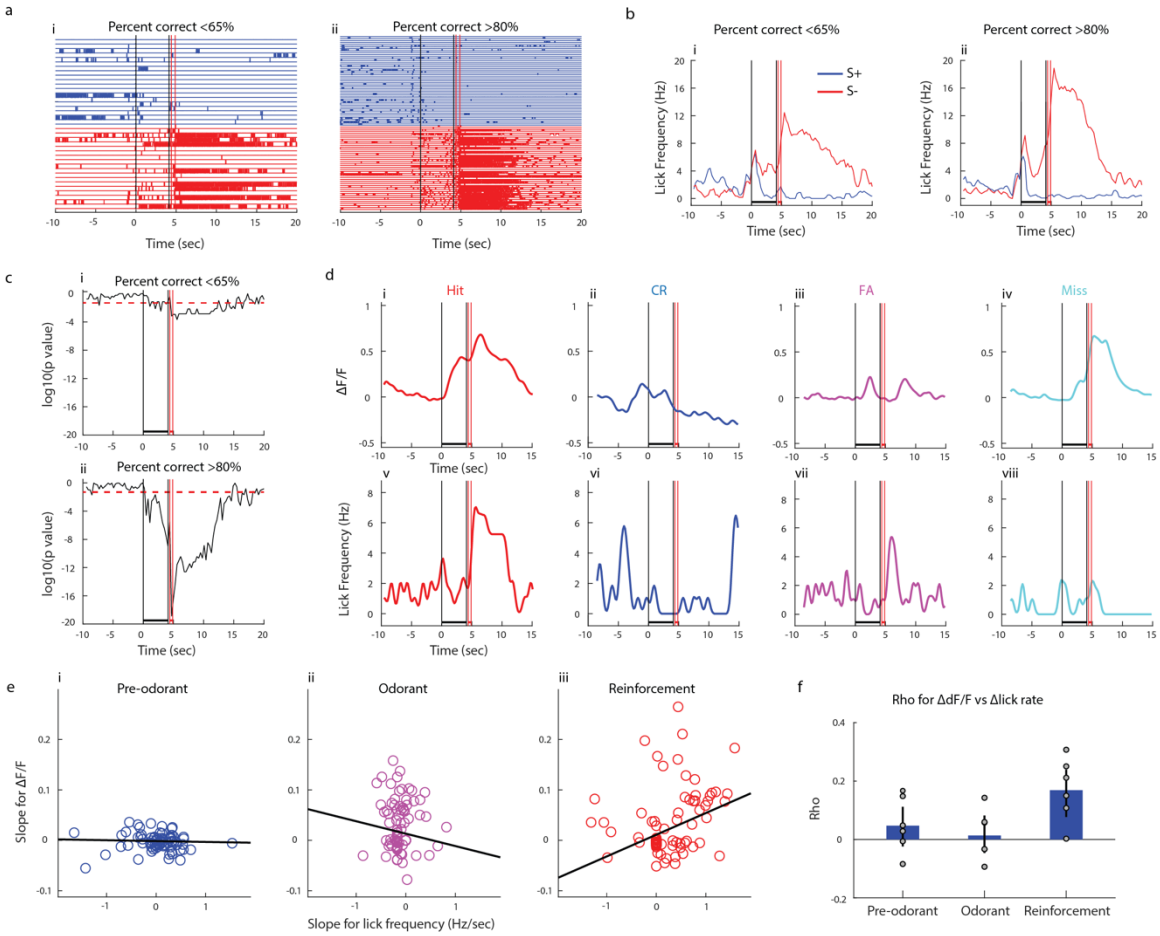

Figure 6. Changes in lick rate correlate with changes in MLI activity during the reinforcement period, but not during the odorant period.

a. Examples of per trial lick traces when the mouse was learning to discriminate the odorants (**i**, <65% correct) and when the animal was proficient (**ii**, >85% correct).

b. Average lick frequency for S+ and S- trials shown in **a** (**i**, <65% correct, **ii**, >85% correct).

c. p value for a ranksum test estimating the difference in licks between the S+ and S- odorants for the example in **a** (**i**, <65% correct, **ii**, >85% correct).

d. Single trial examples of average ΔF/F (**i-iv**) and the corresponding lick frequency (**v-viii**).

e. The correlation between the derivative of average ΔF/F and the derivative of lick frequency shown per time point for all trials in a go-no go session. Time points are segregated within the last second before odorant addition (Pre-odorant), during the last second of odorant addition (Odorant) and during the first second after reward (Reinforcement). Correlation coefficients and p values for these time periods are: Pre: -0.045, 0.57. Odorant: -0.12, 0.14. Reinforcement: 0.37, 0.0000018.

f. Correlation coefficients for the relationship between the derivative of average ΔF/F and the derivative of lick frequency for six sessions (five mice). The correlation coefficient is significantly different between reinforcement and odorant (t test corrected for multiple comparisons $p<pFDR=0.016$, $n=6$).

In b, c and d the vertical black lines are odorant onset and removal and the red lines bound the reinforcement period.

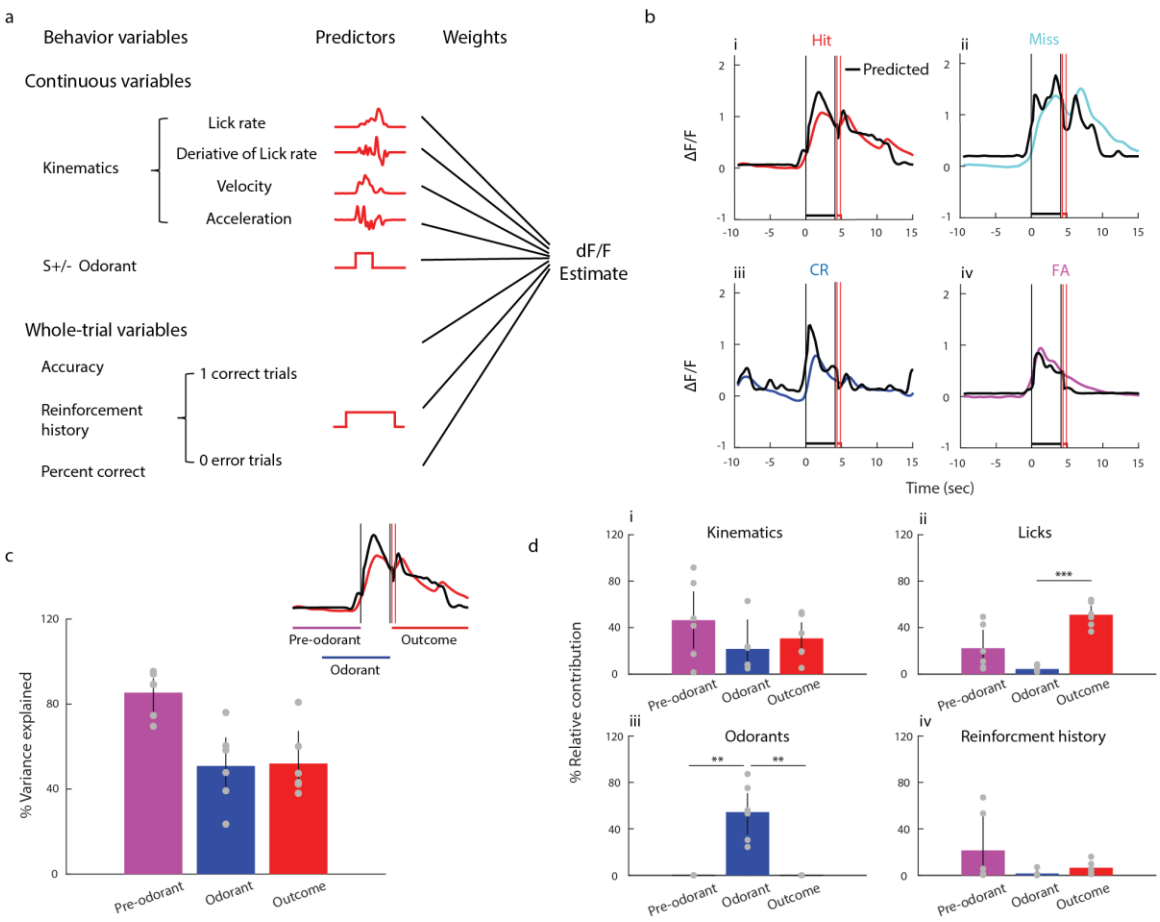

Figure 7. Fit of MLI activity with a generalized linear model (GLM).

a. Schematic illustration of the variables used by the GLM model to quantify the relationship between average ΔF/F and behavioral variables and odorant valence on a per trial basis.

b. Examples of GLM best-fit (black) and actual ΔF/F Ca^{2+} traces for Hit (**i,** red), Miss (**ii**, cyan), CR (**iii**, blue) and FA (**iv**, magenta) trials. The vertical black lines are odorant onset and removal and the red lines bound the reinforcement period.

c. Percent of the variance explained by GLM in the different time periods (Pre-odorant, Odorant and Outcome). The inset shows the time intervals used for the different periods.

d. Relative contribution of kinematics (**i**), licks (**ii**), odorants (**iii**) and reinforcement history (**iv**) to the GLM fit for fits in the different time periods (pre-odor, odor, outcome). The

results showed that odorants and licks play an important role in contributing to the activity during odorants and outcome periods respectively, while kinematics contribute to the activity in all three time periods. Asterisks for Licks (**ii**) and Odorants (**iii**) denote significant differences determined by ranksum and t test ($p<pFDR=0.033$, $n=6$). There are no significant differences for Kinematics (**i**) or Reinforcement history (**iv**) ($p>pFDR=0.017$, ranksum test).

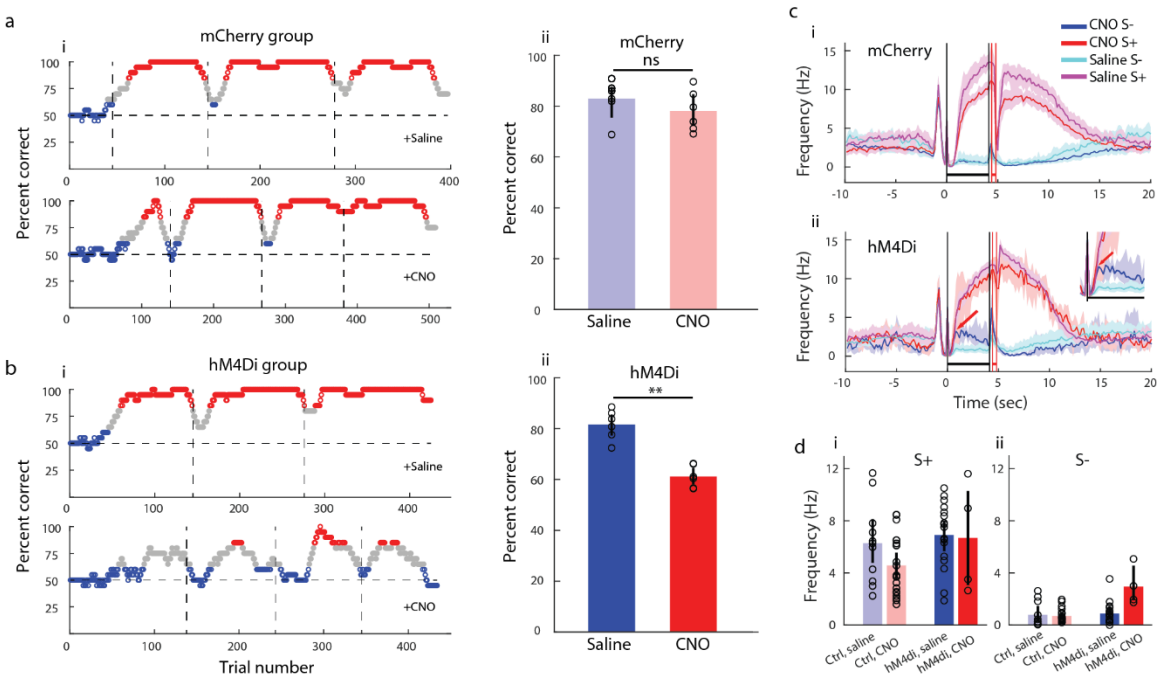

Figure 8. Chemogenetic inhibition of MLI activity impairs associative learning.

a. and b. a,i and b,i. Examples of behavioral performance in a go-no go task where mice learned to differentiate between two odorant mixtures (S+: 0.1% of 60% heptanal+40% ethyl butyrate, S-: 0.1% of 40% heptanal+60% ethyl butyrate). Blue: <=65% correct, red: >80% correct.

a,ii and b,ii. Behavioral performance (mean± 95% CIs, n=6). **a.** Mice expressing mCherry in MLIs. **b.** Mice expressing hM4Di in MLIs. A GLM analysis indicates that there is a statistically significant interaction between CNO drug treatment and hM4Di expression ($p<0.01$, 24 observations, 20 d.f.) and post hoc unpaired t tests corrected for multiple comparisons indicate that the h4DMi expressing group differs between CNO and saline (asterisks, $p<pFDR=0.025$, n=12 mice).

c. Average lick frequency time course for the mCherry (**i**) and hM4Di (**ii**) groups (mean+ 95% CI, shade). The red arrow in the inset shows that for S- trials of CNO treated hM4Di animals (blue), the animal kept licking for a longer time than S- trials for mice injected

with saline (cyan). The vertical black lines are odorant onset and removal and the red lines bound the reinforcement period.

d. Mean lick frequency (±CI) during the initial portion of the odorant application period (0.8 to 1.8 sec) for mice performing >80% correct (**i**: S+, **ii**: S-). GLM analysis did not find a statistically significant difference for treatment or h4DMi expression (or interactions) for S+ ($p>0.05$, 53 observations, 49 d.f.), and found a difference for CNO treatment x h4DMi expression for S- ($p<0.001$, 53 observations, 49 d.f).

Supplementary Information

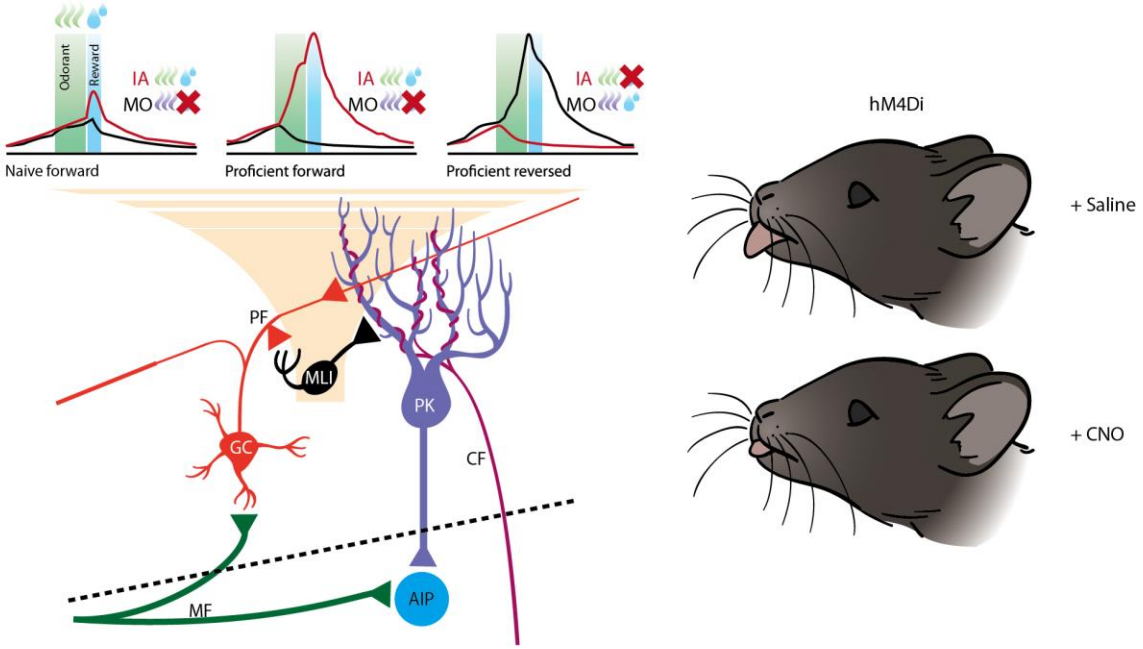

Supplementary Figure 1. Diagram of the cerebellar circuit and summary of the findings. This figure shows the circuit for the cerebellum. Climbing fibers (CFs) innervate the dendrites of Purkinje cells (PCs). Sensorimotor input is conveyed by Mossy fibers (MFs) to granule cells (GCs). The GCs innervate the dendrites of the PCs through parallel fibers (PFs). In this project we study the activity of molecular layer interneurons (MLIs) that receive innervation from GCs and inhibit PCs. We find that the activity of the MLIs reflect the valence of the odorants. Inhibiting MLIs with DREADDs results in decreased ability to respond differentially to the odorants in the go-no go task.

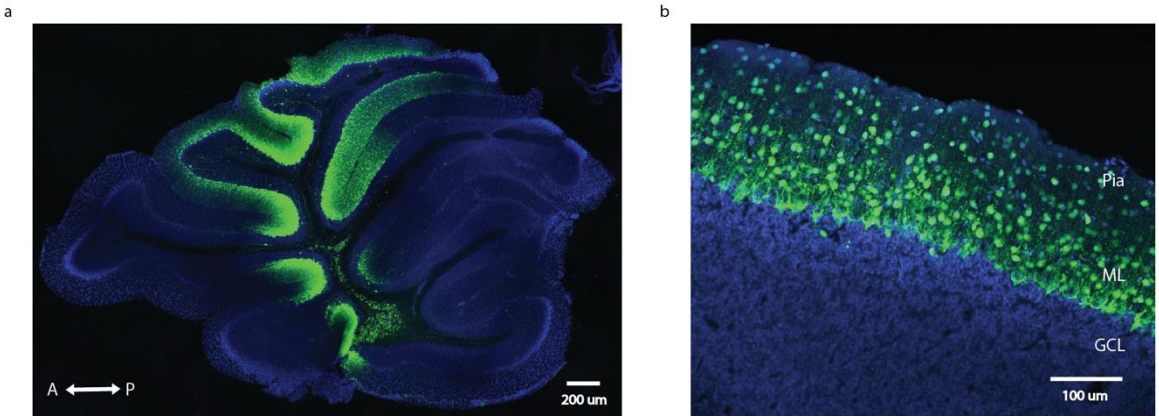

Supplementary Figure 2. Expression of GCaMP6f in fixed tissue slices. GCaMP6f fluorescence in cerebellar sagittal brain slices from PV-Cre mice infected with AAV1-Syn-Flex-GCaMP6f. GCaMP6f (green) is expressed in the MLI layer. The slices were counterstained with DAPI.

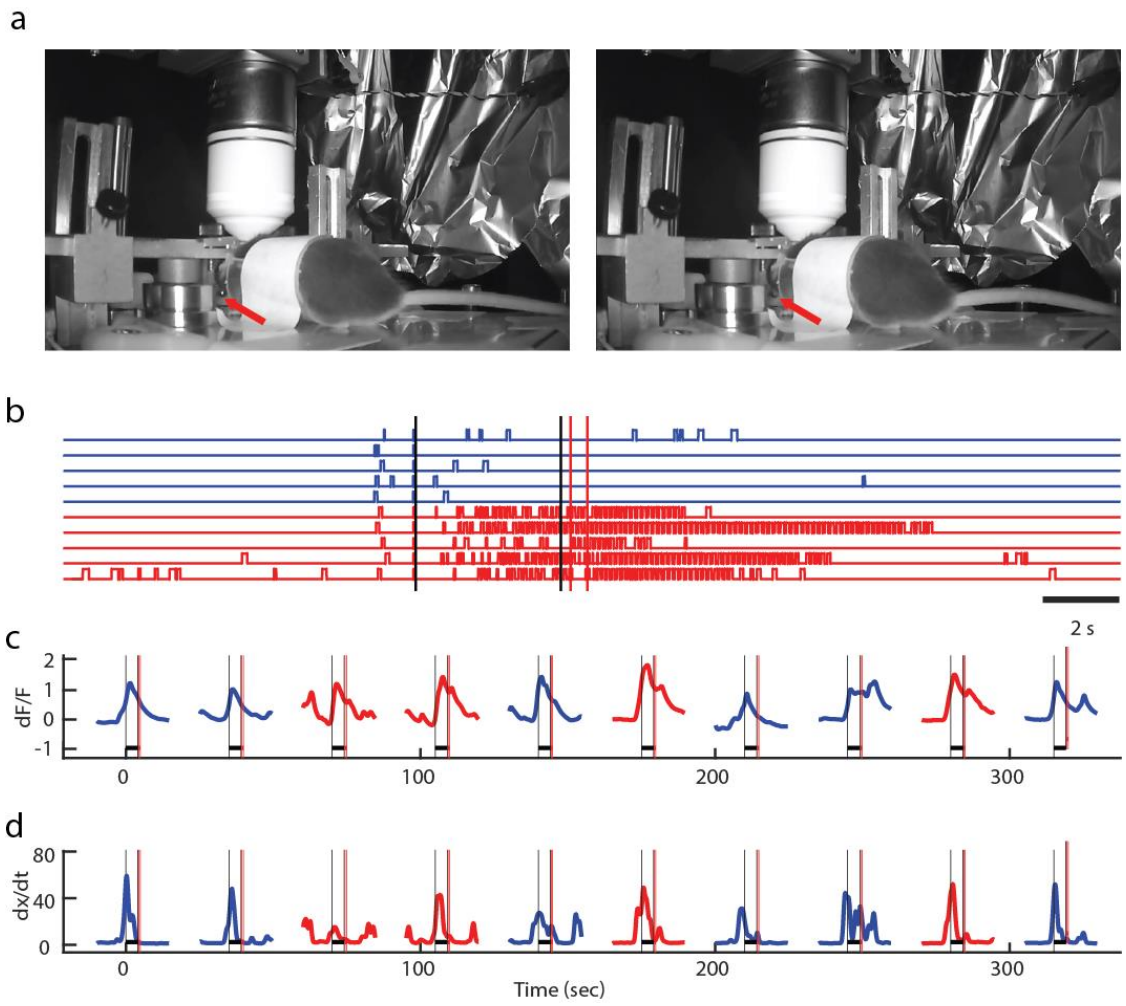

Supplementary Figure 3. Mouse leans into the port and licks on the water spout to initiate the trial.

a. Images show the mouse before (left) and at the start (right) of the trial.

b. Lick traces for a subset of trials for a mouse that was proficient (>80% correct) in the go-no go task. Notice how there is a lick 1-1.5 sec before the odorant is delivered. Red: S+, blue: S-.

c. Examples of ΔF/F Ca^{2+} traces for a subset of trials.

d. Velocity of mouse movement for these trials.

The vertical black lines are odorant onset and removal and the red lines bound the reinforcement period.

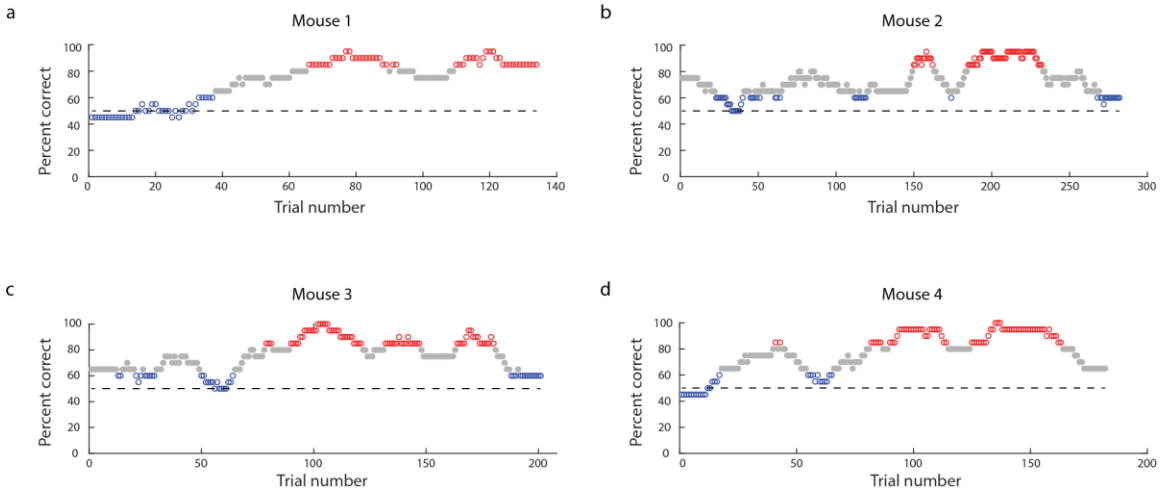

Supplementary Figure 4. Behavioral performance for the mice included in the analysis in Fig. 2g. The plots show percent correct performance for one session for each mouse. Red: percent correct >=80%, blue percent correct <=65%.

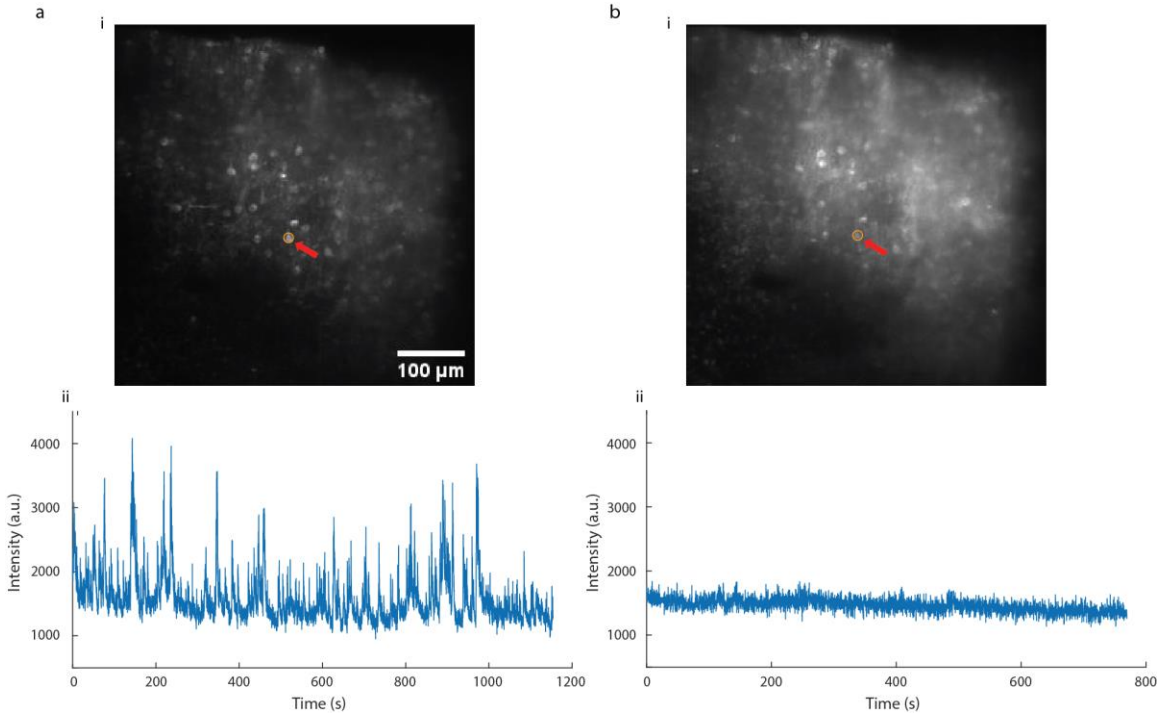

Supplementary Figure 5. Control for axial movement while imaging MLI activity in the animal engaged in the go-no go task. Two photon imaging was performed in the MLI layer of a mouse engaged in the go-no go task with excitation at either 920 nm (a, GCaMP6f emission Ca2+-sensitive) or 820 nm (b, GCaMP6f emission Ca2+-insensitive). Fluorescence transients were detected at 920 nm excitation, but not at 820 nm excitation indicating that the transients were not due to axial movement.

Supplementary Movie 1. The movie shows mouse movement for 25 seconds starting 10 seconds before trial initiation.

1 Cayco-Gajic, N. A. & Silver, R. A. Re-evaluating Circuit Mechanisms Underlying Pattern Separation. *Neuron* **101**, 584-602, doi:10.1016/j.neuron.2019.01.044 (2019).

2 Strick, P. L., Dum, R. P. & Fiez, J. A. Cerebellum and nonmotor function. *Annu Rev Neurosci* **32**, 413-434, doi:10.1146/annurev.neuro.31.060407.125606 (2009).

3 Sokolov, A. A., Miall, R. C. & Ivry, R. B. The Cerebellum: Adaptive Prediction for Movement and Cognition. *Trends Cogn Sci* **21**, 313-332, doi:10.1016/j.tics.2017.02.005 (2017).

4 Adamaszek, M. *et al.* Consensus Paper: Cerebellum and Emotion. *Cerebellum* **16**, 552-576, doi:10.1007/s12311-016-0815-8 (2017).

5 Wang, S. S., Kloth, A. D. & Badura, A. The cerebellum, sensitive periods, and autism. *Neuron* **83**, 518-532, doi:10.1016/j.neuron.2014.07.016 (2014).

6 Jelitai, M., Puggioni, P., Ishikawa, T., Rinaldi, A. & Duguid, I. Dendritic excitation-inhibition balance shapes cerebellar output during motor behaviour. *Nat Commun* **7**, 13722, doi:10.1038/ncomms13722 (2016).

7 Gao, Z., van Beugen, B. J. & De Zeeuw, C. I. Distributed synergistic plasticity and cerebellar learning. *Nat Rev Neurosci* **13**, 619-635, doi:10.1038/nrn3312 (2012).

8 Marr, D. A theory of cerebellar cortex. *J Physiol* **202**, 437-470 (1969).

9 Ito, M. Neural design of the cerebellar motor control system. *Brain Res* **40**, 81-84, doi:10.1016/0006-8993(72)90110-2 (1972).

10 Albus, J. S. A theory of cerebellar function. *Mathematical Biosciences* **10**, 25-61 (1971).

11 Heffley, W. & Hull, C. Classical conditioning drives learned reward prediction signals in climbing fibers across the lateral cerebellum. *Elife* **8**, doi:10.7554/eLife.46764 (2019).

12 Tsutsumi, S. *et al.* Modular organization of cerebellar climbing fiber inputs during goal-directed behavior. *Elife* **8**, doi:10.7554/eLife.47021 (2019).

13 Deverett, B., Koay, S. A., Oostland, M. & Wang, S. S. Cerebellar involvement in an evidence-accumulation decision-making task. *Elife* **7**, doi:10.7554/eLife.36781 (2018).

14 Carta, I., Chen, C. H., Schott, A. L., Dorizan, S. & Khodakhah, K. Cerebellar modulation of the reward circuitry and social behavior. *Science* **363**, doi:10.1126/science.aav0581 (2019).

15 Jorntell, H., Bengtsson, F., Schonewille, M. & De Zeeuw, C. I. Cerebellar molecular layer interneurons - computational properties and roles in learning. *Trends Neurosci* **33**, 524-532, doi:10.1016/j.tins.2010.08.004 (2010).

16 Wulff, P. *et al.* Synaptic inhibition of Purkinje cells mediates consolidation of vestibulo-cerebellar motor learning. *Nat Neurosci* **12**, 1042-1049, doi:10.1038/nn.2348 (2009).

17 ten Brinke, M. M. *et al.* Evolving Models of Pavlovian Conditioning: Cerebellar Cortical Dynamics in Awake Behaving Mice. *Cell Rep* **13**, 1977-1988, doi:10.1016/j.celrep.2015.10.057 (2015).

18 Rowan, M. J. M. *et al.* Graded Control of Climbing-Fiber-Mediated Plasticity and Learning by Inhibition in the Cerebellum. *Neuron* **99**, 999-1015 e1016, doi:10.1016/j.neuron.2018.07.024 (2018).

19 Gire, D. H., Whitesell, J. D., Doucette, W. & Restrepo, D. Information for decision-making and stimulus identification is multiplexed in sensory cortex. *Nat Neurosci* **16**, 991-993, doi:10.1038/nn.3432 (2013).

20 Doucette, W. & Restrepo, D. Profound context-dependent plasticity of mitral cell responses in olfactory bulb. *PLoS Biol* **6**, e258, doi:08-PLBI-RA-1962 [pii] 10.1371/journal.pbio.0060258 (2008).

21 Helmchen, F. & Denk, W. Deep tissue two-photon microscopy. *Nature methods* **2**, 932-940, doi:10.1038/nmeth818 (2005).

22 Chen, T. W. *et al.* Ultrasensitive fluorescent proteins for imaging neuronal activity. *Nature* **499**, 295-300, doi:10.1038/nature12354 (2013).

23 Armbruster, B. N., Li, X., Pausch, M. H., Herlitze, S. & Roth, B. L. Evolving the lock to fit the key to create a family of G protein-coupled receptors potently activated by an inert ligand. *Proc Natl Acad Sci U S A* **104**, 5163-5168, doi:10.1073/pnas.0700293104 (2007).

24 Giovannucci, A. *et al.* Cerebellar granule cells acquire a widespread predictive feedback signal during motor learning. *Nat Neurosci* **20**, 727-734, doi:10.1038/nn.4531 (2017).

25 Wagner, M. J., Kim, T. H., Savall, J., Schnitzer, M. J. & Luo, L. Cerebellar granule cells encode the expectation of reward. *Nature* **544**, 96-100, doi:10.1038/nature21726 (2017).

26 Giovannucci, A. *et al.* CaImAn an open source tool for scalable calcium imaging data analysis. *Elife* **8**, doi:10.7554/eLife.38173 (2019).

27 Litwin-Kumar, A., Harris, K. D., Axel, R., Sompolinsky, H. & Abbott, L. F. Optimal Degrees of Synaptic Connectivity. *Neuron* **93**, 1153-1164.e1157, doi:10.1016/j.neuron.2017.01.030 (2017).

28 Curran-Everett, D. Multiple comparisons: philosophies and illustrations. *Am.J.Physiol Regul.Integr.Comp Physiol* **279**, R1-R8 (2000).

29 Gaffield, M. A. & Christie, J. M. Movement Rate Is Encoded and Influenced by Widespread, Coherent Activity of Cerebellar Molecular Layer Interneurons. *J Neurosci* **37**, 4751-4765, doi:10.1523/JNEUROSCI.0534-17.2017 (2017).

30 Astorga, G. *et al.* Concerted Interneuron Activity in the Cerebellar Molecular Layer During Rhythmic Oromotor Behaviors. *J Neurosci* **37**, 11455-11468, doi:10.1523/JNEUROSCI.1091-17.2017 (2017).

31 Engelhard, B. *et al.* Specialized coding of sensory, motor and cognitive variables in VTA dopamine neurons. *Nature* **570**, 509-513, doi:10.1038/s41586-019-1261-9 (2019).

32 Gomez, J. L. *et al.* Chemogenetics revealed: DREADD occupancy and activation via converted clozapine. *Science* **357**, 503-507, doi:10.1126/science.aan2475 (2017).

33 Raymond, J. L. & Medina, J. F. Computational Principles of Supervised Learning in the Cerebellum. *Annu Rev Neurosci* **41**, 233-253, doi:10.1146/annurev-neuro-080317-061948 (2018).

34 Davie, J. T., Clark, B. A. & Hausser, M. The origin of the complex spike in cerebellar Purkinje cells. *J Neurosci* **28**, 7599-7609, doi:10.1523/JNEUROSCI.0559-08.2008 (2008).

35 Otsu, Y. *et al.* Activity-dependent gating of calcium spikes by A-type K+ channels controls climbing fiber signaling in Purkinje cell dendrites. *Neuron* **84**, 137-151, doi:10.1016/j.neuron.2014.08.035 (2014).

36 Rancz, E. A. & Hausser, M. Dendritic calcium spikes are tunable triggers of cannabinoid release and short-term synaptic plasticity in cerebellar Purkinje

neurons. *J Neurosci* **26**, 5428-5437, doi:10.1523/JNEUROSCI.5284-05.2006 (2006).

37 Finch, E. A., Tanaka, K. & Augustine, G. J. Calcium as a trigger for cerebellar long-term synaptic depression. *Cerebellum* **11**, 706-717, doi:10.1007/s12311-011-0314-x (2012).

38 Linden, D. J. & Connor, J. A. Long-term synaptic depression. *Annu Rev Neurosci* **18**, 319-357, doi:10.1146/annurev.ne.18.030195.001535 (1995).

39 Eccles, J. C., Llinas, R. & Sasaki, K. The excitatory synaptic action of climbing fibres on the Purkinje cells of the cerebellum. *J Physiol* **182**, 268-296, doi:10.1113/jphysiol.1966.sp007824 (1966).

40 Brown, A. M. *et al.* Molecular layer interneurons shape the spike activity of cerebellar Purkinje cells. *Sci Rep* **9**, 1742, doi:10.1038/s41598-018-38264-1 (2019).

41 Gaffield, M. A., Rowan, M. J. M., Amat, S. B., Hirai, H. & Christie, J. M. Inhibition gates supralinear Ca(2+) signaling in Purkinje cell dendrites during practiced movements. *Elife* **7**, doi:10.7554/eLife.36246 (2018).

42 Jorntell, H. & Ekerot, C. F. Receptive Field Remodeling Induced by Skin Stimulation in Cerebellar Neurons in vivo. *Front Neural Circuits* **5**, 3, doi:10.3389/fncir.2011.00003 (2011).

43 Dean, H. L., Hagan, M. A. & Pesaran, B. Only coherent spiking in posterior parietal cortex coordinates looking and reaching. *Neuron* **73**, 829-841, doi:10.1016/j.neuron.2011.12.035 (2012).

44 Lennon, W., Yamazaki, T. & Hecht-Nielsen, R. A Model of In vitro Plasticity at the Parallel Fiber-Molecular Layer Interneuron Synapses. *Front Comput Neurosci* **9**, 150, doi:10.3389/fncom.2015.00150 (2015).

45 Szapiro, G. & Barbour, B. Multiple climbing fibers signal to molecular layer interneurons exclusively via glutamate spillover. *Nat Neurosci* **10**, 735-742, doi:10.1038/nn1907 (2007).

46 Chabrol, F. P., Blot, A. & Mrsic-Flogel, T. D. Cerebellar Contribution to Preparatory Activity in Motor Neocortex. *Neuron* **103**, 506-519 e504, doi:10.1016/j.neuron.2019.05.022 (2019).

47 Hernandez-Briones, Z. S. *et al.* Olfactory stimulation induces cerebellar vermis activation during sexual learning in male rats. *Neurobiol Learn Mem* **146**, 31-36, doi:10.1016/j.nlm.2017.11.003 (2017).

48 Sobel, N. *et al.* Odorant-induced and sniff-induced activation in the cerebellum of the human. *J Neurosci* **18**, 8990-9001 (1998).

49 Mainland, J. D., Johnson, B. N., Khan, R., Ivry, R. B. & Sobel, N. Olfactory impairments in patients with unilateral cerebellar lesions are selective to inputs from the contralesional nostril. *J Neurosci* **25**, 6362-6371, doi:10.1523/JNEUROSCI.0920-05.2005 (2005).

50 Astorga, G. *et al.* An excitatory GABA loop operating in vivo. *Front Cell Neurosci* **9**, 275, doi:10.3389/fncel.2015.00275 (2015).

51 Kuhn, B., Ozden, I., Lampi, Y., Hasan, M. T. & Wang, S. S. An amplified promoter system for targeted expression of calcium indicator proteins in the cerebellar cortex. *Front Neural Circuits* **6**, 49, doi:10.3389/fncir.2012.00049 (2012).

52 Li, A., Gire, D. H. & Restrepo, D. Y spike-field coherence in a population of olfactory bulb neurons differentiates between odors irrespective of associated outcome. *J Neurosci* **35**, 5808-5822, doi:10.1523/JNEUROSCI.4003-14.2015 (2015).

53 Farneback, G. Two-frame motion estimation based on polynomial expansion. *Proceedings of the 13th Scandinavian Conference on Image Analysis*, 363-370 (2003).

54 Barnett, L. M., Hughes, T. E. & Drobizhev, M. Deciphering the molecular mechanism responsible for GCaMP6m's Ca2+-dependent change in fluorescence. *PLoS One* **12**, e0170934, doi:10.1371/journal.pone.0170934 (2017).

55 Litwin-Kumar, A., Harris, K. D., Axel, R., Sompolinsky, H. & Abbott, L. F. Optimal Degrees of Synaptic Connectivity. *Neuron* **93**, 1153-1164 e1157, doi:10.1016/j.neuron.2017.01.030 (2017).